Final Report for Award #G16AP00010

Project Title: Feasibility of Controlling Induced Earthquakes: Seismicity Investigation coupled with Hydrologic Modeling of an Actively Mitigated Class II Disposal Well and Data Collection at New High Rate Wells, Weld County, Colorado

Principal Investigators:

Dr. Anne F. Sheehan
Cooperative Institute for Research in Environmental Sciences (CIRES) and Department of Geological Sciences
University of Colorado Boulder, UCB 399
Boulder, Colorado 80309
Telephone: (303)492-4597
Anne.Sheehan@colorado.edu

Dr. Shemin Ge
Department of Geological Sciences, UCB 399
University of Colorado Boulder
Boulder, Colorado 80309
Telephone: (303)492-8323
Shemin.Ge@colorado.edu

Name of Recipient:
University of Colorado Boulder
Office of Contracts and Grants
3100 Marine Street, ARC
572 UCB
Boulder, Colorado 80309-0572
P (303)492-6221

Dates covered by this award:
January 1, 2016 – December 31, 2017

Abstract

We performed combined seismicity and hydrologic studies of an actively mitigated high rate Class II wastewater disposal well and several new high rate wells in northeast Colorado. We 1) deployed seismometers and monitored seismicity at a Class II wastewater injection well where active mitigation has been attempted through shut-in, well modification, staged return to pre-earthquake injection levels, and complicated through addition of a new well less than 1 km away; 2) deployed seismometers near new injection wells throughout NE Colorado in order to characterize background seismicity and potentially capture the onset of seismicity; and 3) performed pore pressure modeling to test the effectiveness of the induced seismicity mitigation. Our seismicity results show a general trend of decreasing seismicity with time after well mitigation attempts in June 2014, an abrupt but temporary increase in seismicity in August 2016 after a new injection well was put in operation near the epicenter of the induced earthquakes, and no seismicity to date at more distant new injection wells. We performed pore pressure modeling using injection, geologic, and seismicity data. Results from the hydrologic modeling show the influence of injection on pore pressure at short distances from the earthquakes but also the significant contribution to pore pressure change by injection at all distances modeled, up to 30 km, from the earthquake. In order to have appropriate parameters to use for the hydrologic modeling, we conducted constant-head permeameter tests on samples collected from core drilled in the DJ Basin and stored at the USGS CRC in Denver, Colorado. The core samples are from the 1 UPPR-Ferch Well that was cored through all of the geologic units of the Denver Basin combined disposal zone. We took samples from the Lyons, Wolfcamp, Ingleside, and Fountain Formations.

Introduction

On May 31, 2014 (June 1 UTC) a magnitude 3.2 earthquake occurred east of Greeley, Colorado, in Weld County, northeast Colorado (Figure 1). Weld County has been the locus of significant oil and gas production in the past decade, and hosts many Class II injection wells to dispose of wastewater generated from oil and natural gas production and drilling activities. Weld County had not had any noticeable seismicity in the past. The May 31 earthquake was widely felt, with felt reports from Boulder and Golden, over 60 miles away from the epicenter. The epicenter was close to a high volume injection well that was quite deep (nearly to basement) and was also less than a year old. In response to the earthquake, Sheehan's research group at the University of Colorado (CU) deployed six seismometers and one accelerometer beginning three days after the earthquake. Earthquakes were located in a small cluster (~2 km radius) centered near a Class II injection well (NGL Well C4A). The injection company, NGL Energy Partners LP, had been injecting waste fluid into the deepest sedimentary formation of the Denver Basin at rates as high as 360,000 barrels/month for less than a year. The earthquake and subsequent seismicity sequence recorded by the CU team contributed to the decision by the Colorado Oil and Gas Conservation Commission (COGCC) to recommend a temporary halt to injection at well NGL C4A. The C4A well data, drilling logs, and well files, were reviewed. The drilling logs indicated several lost circulation zones in the bottom several hundred feet of the well. The well was drilled into the Fountain Formation, which is in immediate contact with crystalline basement. A spinner test (measures fluid flow velocity in well based on the speed of rotation of a fan-like 'spinner') conducted by the operator indicated that most of the flow was in the highly fractured zone at the bottom of the well. As a result of the test and the recommendation of the COGCC, the operator (NGL) plugged back the well approximately 458 feet. Injection resumed at 5000 bpd (barrels per day) on July 19, 2014 with injection increasing to 7500 bpd in August 2014 and again in October 2014 to 9500 bpd. The increased injection volumes were allowed by COGCC with review of the University of Colorado seismic monitoring data. The well has now reached injection rates of 10000 bpd, and has not exceeded the pre-earthquake high rates of 12000 bpd. However, in April 2015, a new Class II wastewater disposal well, EWS-2, came into operation within a kilometer of the NGL C4A well, further complicating the potentially delicate balance between injection and earthquakes. In June 2016, the combined EWS-2 and NGL-C4A injection rates exceeded 500,000 barrels/month, and several felt earthquakes occurred in August 2016. In response to the earthquakes the wells were temporarily shut-in (taken out of operation), and the mitigation similar to that at NGL-C4A (cementing the bottom of the well) was expanded to EWS-2 and nearby HPD Kersey 1.

a)

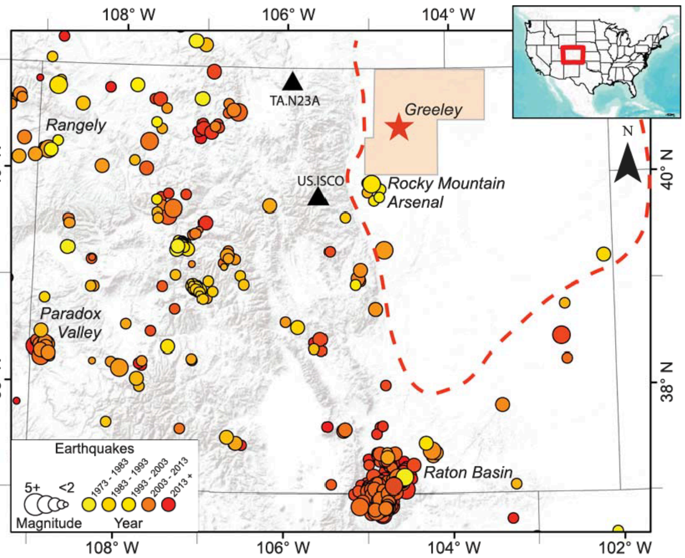

Figure 1. Seismicity of Colorado (circles) as compared to the location of the Weld County 1June2014 earthquake (red star). The approximate boundaries of the Denver-Julesburg Basin (red dashed line) and Weld County (orange shaded region) are shown. The nearest coeval stations to the 1June earthquake, US.ISCO and TA.N23A, are show as black triangles. Other notable regions of documented induced seismicity in Colorado are labeled, including Rocky Mountain Arsenal, Rangely, Paradox Valley, and Raton Basin. Seismicity are from USGS ANSS catalog.

Our work during this grant period included seismic data collection near wells C4A and EWS-2, analysis of the seismic data collected, development of subsurface hydraulic parameters through reanalysis of step rate tests, laboratory analysis of core samples of disposal zone rocks, hydrologic modeling that combines C4A injection data with seismicity observations, and seismic data collection at 10 new high rate injection wells or groups of wells in Weld County.

Rapid Response and Mitigation of Induced Seismicity (excerpts from Yeck et al., SRL, 2016)

Our group responded rapidly to the 2014 Greeley Mw3.2 earthquake, deploying a 6 station seismograph network around the epicenter. Equipment was from the IRIS PASSCAL Rapid Array Mobilization Program (RAMP). Six seismic stations (network code XU 2014-2015) were deployed, the first of which the University of Colorado deployed on June 04, 2014, three days after the Greeley M_w 3.2 earthquake. Instrumentation included six short-period (Sercel L-22) 3-

component seismometers, one Episensor 3-component strong motion instrument, and Reftek 130 data loggers for all. Seismometers were deployed surrounding the estimated location of the Greeley M_w 3.2 earthquake (Figure 2). The first temporary seismic station was installed June 3rd, 2 days after the June 1st Greeley earthquake.

The USGS-determined epicentral location of the Greeley M_w 3.2 earthquake had a large uncertainty (~6 km) due to the network geometry at the time of the earthquake, and consequently, the temporary stations were originally deployed as a large (~15 km circumradius) triangle to ensure encompassing the Greeley M_w 3.2 earthquake epicenter (stations GRNE, GRNW, GRSO), with two stations placed near the epicenter (stations GREP and GRES) (Figure 2). Station GREP was placed closest to our estimate of the Greeley M_w 3.2 earthquake epicenter, based on the original reported location of the earthquake and descriptions of the earthquake from nearby residents. After initial hypocenters of microseismicity were computed, GRNW was moved to station GRWE, as no earthquakes were observed near GRNW. GRCO was added to the network a few months after the initial deployment to help constrain depths of observed earthquakes.

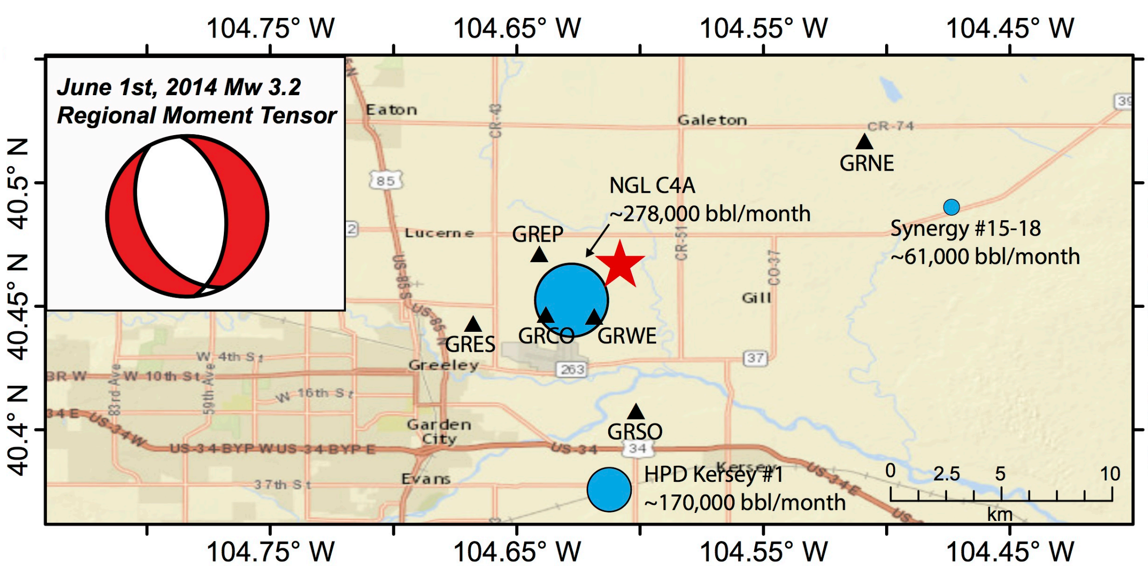

Figure 2. Map showing the location of the June 1st earthquake epicenter (red star), initially reported by the USGS NEIC, as compared to nearby wastewater disposal wells (blue circles) and temporary seismic stations (black triangles) deployed after Greeley M_w 3.2 earthquake. Temporally deployed XU station GRNW not shown. Injection well symbol sized by one-year average of monthly reported injection rates prior to Greeley mainshock (reported rates available at http://cogcc.state.co.us/). Focal mechanism of June 1st Greeley M_w 3.2 earthquake is shown in the top left corner (Herrmann, 2016).

In order to search for seismicity prior to the deployment of our local network, we performed subspace detection using two stations, US.ISCO and TA.N23A, both of which recorded the Greeley M_w 3.2 earthquake and two subsequent earthquakes with $M_L > 2$ at high fidelity. We use 25-second, 3-component waveform templates of these high-quality recordings, incorporating the direct P arrival through a portion of the S wave coda, bandpass filtered between 0.8 and 3 Hz. This filter range was selected through trial and error in an effort to enhance the signal-to-noise ratio (SNR). Approximate magnitudes for detected earthquakes are calculated from the ratio of maximum amplitudes to those recorded from the M_w 3.2 Greeley earthquake, thereby estimating a relative magnitude based on the M_L formulation for magnitude. We ran the detector at both US.ISCO and TA.N23A for a four-year period (May 2011 – May 2015) (Figure 2). We required detection at both stations to declare an event. In total, we detected 54 earthquakes, all with similar waveforms (Figure 3). Thirty-one earthquakes were detected prior to the Greeley M_w 3.2 earthquake, the earliest of which occurred on November 7th 2013 (Figure 3), roughly four months after the start of high-rate injection at the C4A well. No events were detected prior to November 2013.

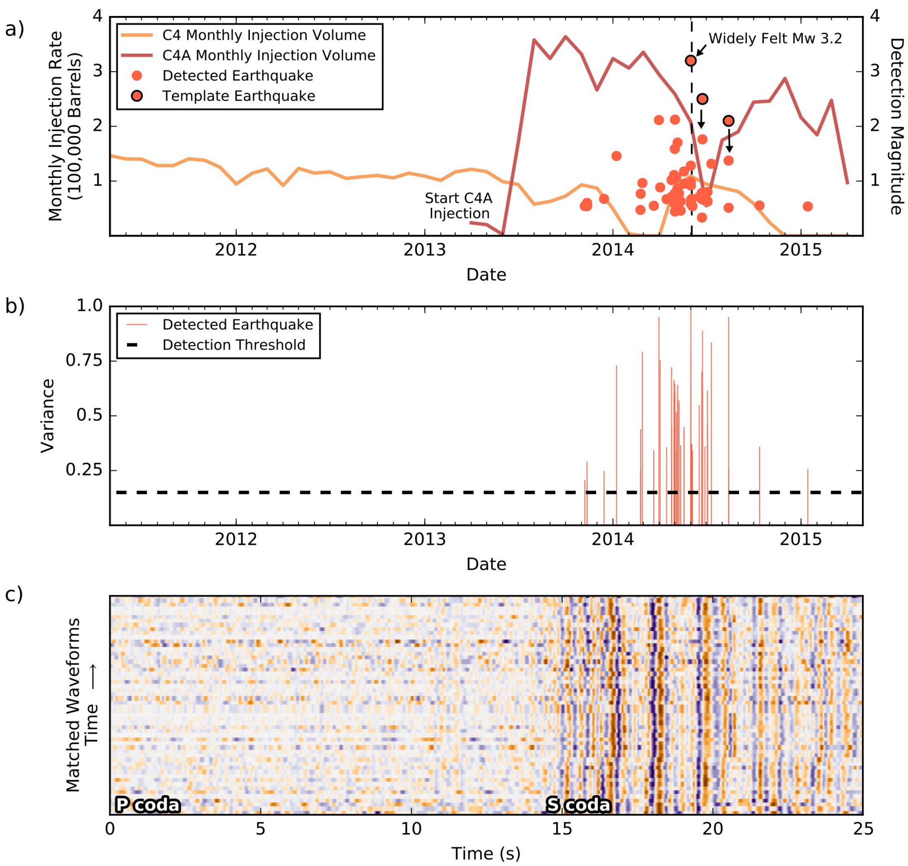

Figure 3: a) Jointly detected earthquakes (red circles) from subspace detectors at nearest seismic stations prior to our temporary deployment (US.ISCO and TA.N23A, ~110 km away). Reported monthly injection volumes for C4 (orange) and C4A (red) wastewater disposal wells shown. No earthquakes were detected prior to the start of high-volume C4A injection. Detected earthquakes increase in magnitude until the largest (M_w 3.2) event. Dashed black line shows date of the first deployed local seismic station. Arrows connect template events with USGS-reported magnitudes to magnitudes calculated relative to M_w 3.2 earthquake amplitudes, which suggests large uncertainties or bias in detection magnitudes. b) Detected earthquake waveform correlation with template (red line) as compared to the detection threshold (dashed line). c) Normalized seismic waveforms shown for detected events, sorted by time of detection. The Greeley template was 25 seconds long, incorporating the P and S wave codas.

The NGL Water Solutions (NGL) C4A Class-II wastewater disposal well (C4A) was both the closest well to the Greeley earthquake epicenter and the highest rate injection well in northeast Colorado in the previous year (Figure 3). C4A injection rates exceeded 250,000 (maximum 363,888) barrels/month since August 2013 at a depth within ~200 meters of the sediment-basement contact (Figure 4). Logging reports of the C4A well show that the rate of penetration of the drill bit when drilling the well increased substantially in middle-lower Fountain Formation, in conjunction with a loss of circulation when drilling. The observations suggest the mid-lower Fountain Formation is highly fractured and highly permeable. This was corroborated by a spinner survey, a measure of fluid velocity as a function of depth that found the majority of injected fluid was entering the bottom of the injection interval. A highly fractured lower Fountain Formation could suggest substantial hydraulic interaction with the Precambrian basement.

In an attempt to mitigate the potential induced seismicity, the C4A well was shut-in, its bottom cemented in, and then injection was reintroduced in a staged manner. NGL cemented the bottom 500 ft. (152.4 m) of the well in an effort to inhibit the hydraulic connection between injection and the crystalline basement and thus reduce the risk of inducing earthquakes. The cement plug filled the portion of the well within the potentially highly fractured and permeable section of Fountain Formation. As the collocated C4 well historically had safely injected at a lower rate into shallower formations, the cementing in of the deeper part of C4A was an attempt to reduce the potential of future induced earthquakes. Injection resumed one month later and injection rates were incrementally increased, starting at 5,000 barrels (bbls) per day on July 19th 2014, increasing to 7,500 bbls/day August 7th, 9,500 bbls/day October 3rd, and finally increasing to 12,000 bbls/day on December 10th 2014.

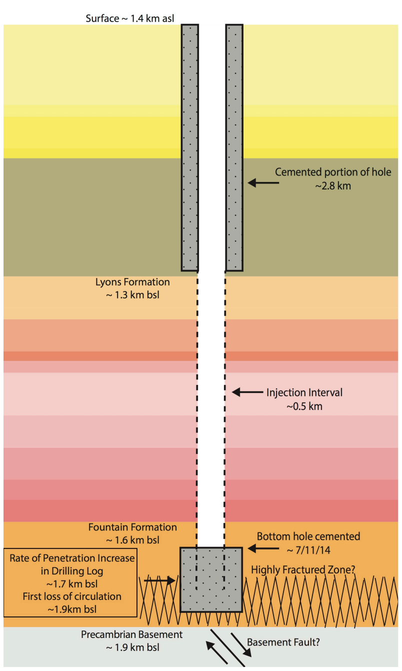

Figure 4. Simplified schematic of C4A wastewater disposal well, adapted from COGCC schematic (http://ogccweblink.state.co.us/DownloadDocument.aspx?DocumentId=3398903). Rate of penetration and loss of circulation observations are from logs available on COGCC website (http://ogccweblink.state.co.us/DownloadDocument.aspx?DocumentId=3055907). The presence of a normal basement fault inferred from regional moment tensor of the June 1st 2014 M_w 3.2 earthquake. A highly fractured zone in the lower Fountain Formation inferred from the increase in the rate of penetration and a subsequent loss of circulation in the drilling report. Schematic shows portion of the bottom hole cemented as a mitigation effort following the M_w 3.2 earthquake.

We detected numerous earthquakes on our temporary seismic network using both standard short-term average/long-term average (STA/LTA) pickers and subspace detection. STA/LTA pickers and visual inspection were used to locate high SNR earthquakes, which we then used to create a suite of subspace detectors for individual stations. We built detectors using all three components for each of the high quality stations GRWE, GRCO, GREP, and GRES. Because event-station distances are small, we use 3-second templates bandpass filtered between 8 and 16 Hz. We associated detections from each station into events by requiring time-coincident (within 2.5 seconds) detections at a minimum of three stations. Using this process we were able to detect and locate 643 earthquakes between 2014/06/06 and 2015/04/27. Magnitudes were calculated using the correlation magnitude formulation defined by Benz et al. [2015], and we report networked-average magnitudes for detected events, including standard errors when three or more stations detected an earthquake. Detection magnitudes were computed relative to a July 10th M_L 2.1 earthquake.

During our local seismic deployment, the rate of seismicity was largest in the months following the Greeley M_w 3.2 earthquake (Figure 5), and with the exception of a few sequences of events, has remained low following mitigation efforts. Our ability to detect earthquakes increased with the installation of station GRWE (June 20th 2014); we observed more seismicity directly after the installation of this station (Figure 5). Of the earthquakes recorded in the months following the M_w 3.2 event, most occurred as part of two small earthquake swarms in January and April 2015. We detected only six earthquakes with magnitudes greater than 1.5, the last of which occurred in August of 2014. With the exception of the clusters of earthquakes in January and April 2015, seismic rates of relatively larger events have remained low in agreement with our observations from subspace detection at distant stations (Figure 2). Through December 2015, no earthquakes exceeded M 1.5. The catalog has a magnitude of completeness of 0.0 estimated using the point of maximum curvature of the frequency-magnitude distribution [*Wiemer and Wyss*, 2000; *Wiemer*, 2001].

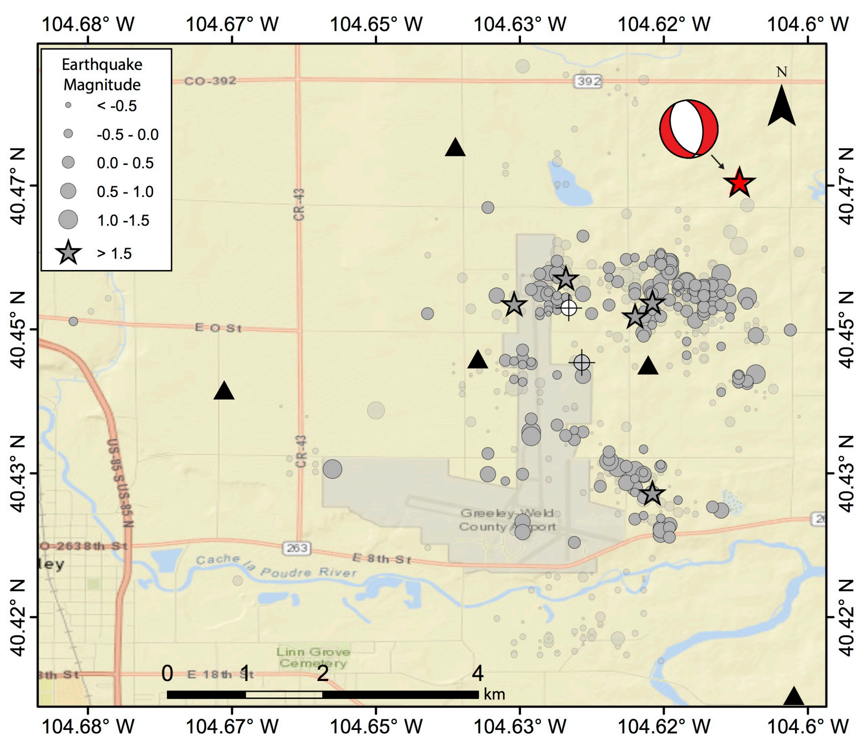

Figure 5 - Map of earthquakes detected and located from our temporary deployment. Earthquakes (gray circles) sized by magnitude. Earthquakes with M > 1.5 are shown as gray stars. Earthquakes with maximum horizontal errors larger than 0.5 km are shown as lighter gray. Red star denotes the USGS NEIC location of the M_w 3.2 Greeley earthquake (prior to local seismic station deployment) and its focal mechanism is shown. The location of the C4A well top (white) and bottom (gray) are shown as circles with crosses. Local seismic stations are shown as black triangles.

We used the non-linearized earthquake location algorithm, *NonLinLoc*, [*Lomax et al.*, 2000, 2009] to locate the earthquakes. *NonLinLoc* uses a global search to calculate probabilistic earthquake locations. We use a six-layer 1D crustal velocity model based on reported models used in studies of the Rocky Mountain Arsenal [*Healy*, 1966] and local well logs (Table 1). The small amplitudes of the earthquakes (most earthquakes were < magnitude 1.0) and high cultural noise in the region limited the number of high-quality picks at distant stations, GRNE and GRSO, thus reducing the azimuthal coverage of many detected earthquakes and resulting in larger location uncertainties.

Of the 643 earthquakes, 190 earthquakes have maximum horizontal uncertainties (68% confidence) of less than 0.5 km, and 359 have vertical uncertainties of less than 0.5 km. Earthquakes with maximum horizontal uncertainties less than 0.5 km show some spatial clustering of earthquakes (Figure 6). A possible northwest-trending lineation of microseismicity is present in the southern portion of the seismicity cluster. The strike of this lineation agrees witha strike of the fault plane modeled from the regional moment tensor solution of the M_w 3.2 earthquake. However, the microseismicity uncertainties are generally too large to clearly define such a feature. The majority of earthquake hypocenters were located in the crystalline Precambrian basement, ~1–2 km below the bottom of the injection interval of the C4A well (Figure 7). Most of these earthquakes appear at a depth of ~4.25 km below sea level (bsl), which is consistent with the 5 km depth of the Greeley M_w 3.2 earthquake determined from the regional moment tensor solution. A few small clusters of earthquakes appear at shallower depths farther from the well, still within the Precambrian basement (Figure 6). Shallow earthquakes (~0.5 km bsl) are present, but the depths of these events are poorly constrained (Figure 6).

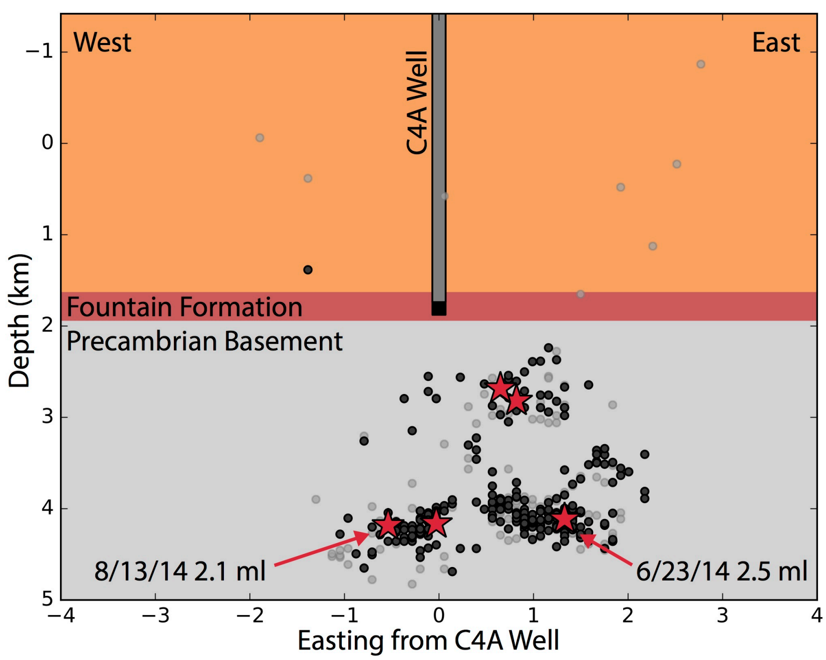

Figure 6 - East-west cross section centered at the top of the C4A well for events at similar latitude as the C4A well (between 40.44° and 40.465°). Black circles denote earthquakes with average depth uncertainties of <0.5 km (68% confidence). Gray circles denote earthquakes with larger errors. The Fountain Formation, the major injection interval of the well, and the Precambrian basement locations are shown. Earthquakes with detection magnitudes >1.5 are denoted as red stars.

Hydrologeologic Modeling (excerpts from Brown et al., JGR, 2017)

Mitigation of injection-induced seismicity in Greeley, Colorado, is based largely on proximity of wastewater disposal wells to seismicity and consists of cementation of the bottom of wells to eliminate connection between the disposal interval and crystalline basement. Brief injection rate reductions followed felt events, but injection rates returned to high levels, >250,000 barrels/month, within six months. While brief rate reduction reduces seismicity in the short term, overall seismicity is not reduced. We examined contributions to pore pressure change by injection from twenty-two wells within 30 kilometers of the center of seismicity. The combined injection rate of seven disposal wells within 15 kilometers of the seismicity (Greeley Wells) is correlated with the seismicity rate. We find that injection from NGL-C4A, the well previously suspected as the likely cause of the induced seismicity, is responsible for ~28% of pore pressure increase. The other six Greeley Wells contribute ~28% of pore pressure increase, and the fifteen Far-field Wells between 15 and 30 kilometers from the seismicity contribute ~44% of pore pressure increase. Modeling results show that NGL-C4A plays the largest role in increased pore pressure, but shows the six other Greeley Wells have approximately the same influence as NGL-C4A. Furthermore, the fifteen Far-field Wells have significant influence on pore pressure near the seismicity.

We used numerical groundwater models to determine if the mitigation efforts were effective. We modeled the pore pressure change caused by injection from 22 wastewater injection wells within 30 km of the seismicity to determine the relative contribution of injection of Greeley Wells close to the seismicity (< 15 km) and the Far-field Wells farther from the seismicity (15 – 30 km). The change in the injection interval caused by the cementing the bottom of the well, the main mitigation action, is also captured during the modeling.

In 2016, there were over 30 disposal wells near Greeley (Figure 7) injecting into the Denver Basin combined disposal zone. The Denver Basin combined disposal zone is a sedimentary interval of approximately 500-meter thick, comprised of the Permian Lyons sandstone Formation, the interbedded sandstone and carbonate Wolfcamp and Ingleside Formations, and the Pennsylvanian Fountain coarse-grained arkose Formation. The Denver Basin combined disposal zone is directly underlain by the Precambrian crystalline basement. A small number of the disposal wells (six) inject into only the upper Denver Basin combined disposal zone (Lyons Formation), while the majority of the disposal wells inject into the entire disposal zone (Lyons through Fountain Formations).

Taking into account all the wells within 30 km of the seismicity, the total injection rate has been over 1 million bbls/month since 2009 and consistently over two million bbls/month since 2012 (Figure 8a). Between the start of injection at NGL-C4A and the June 2014 earthquake, the averaged total injection rate for all wells was approximately three million bbls/month. Between June 2014 and August 2016, when another felt sequence of earthquakes occurred, the average injection rate for all wells has been over four million bbls/month.

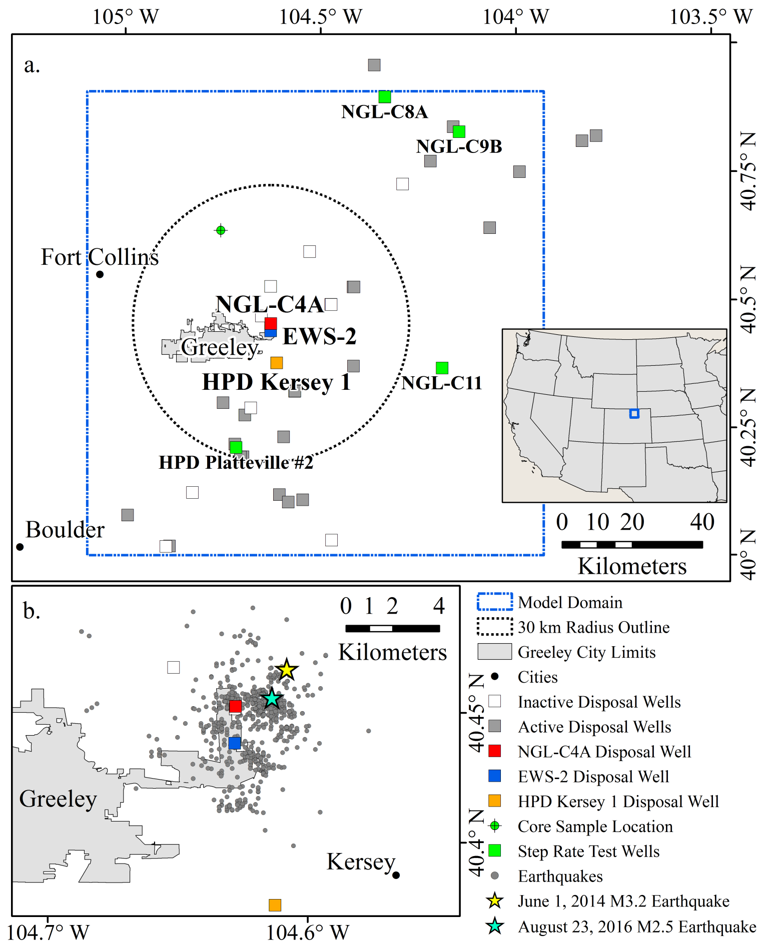

Figure 7: Study area. (a.) Wastewater disposal wells (squares) within Weld County, Colorado. Disposal Wells that were involved in mitigation efforts are NGL-C4A in red, EWS-2 in blue, and HPD Kersey 1 in orange. Step Rate Test reanalysis wells are marked in green. The well location for the core used in constant-head permeameter tests is marked in green circle with cross. The model domain is outlined in dashed-blue, and the 30 km radius circle centered on the center of seismicity is in dashed-black. (b.) Seismicity from June 2014 to August 2016. Yellow star indicates the location of the June 1, 2014 M_w 3.2 earthquake and the blue star indicated the location of the felt earthquakes on August 23, 2016. Earthquake data between November 2013 and April 2015 are from *Yeck et al.* [2016].

Seismicity in the area visually correlates with the injection rate of the seven Greeley Wells that are within 15 km of the seismicity with only short time lags of approximately a few months between the peak injection months and increased seismicity (Figure 8b). The data are for the entire period over which both the injection data and seismicity data are available. Seismicity began in November 2013 [*Yeck et al.,* 2016], and continues through the present. Seismicity decreased after the felt sequence in June 2014 corresponding with the decreased injection rates. Seismicity increased again in January 2015, shortly after the injection of the Greeley Wells exceeded 500,000 bbls/month. Another peak in seismicity occurred in April 2015, shortly after injection reached 490,000 bbls/month. Spatially, there is not a clear diffusion front in the seismicity migration.

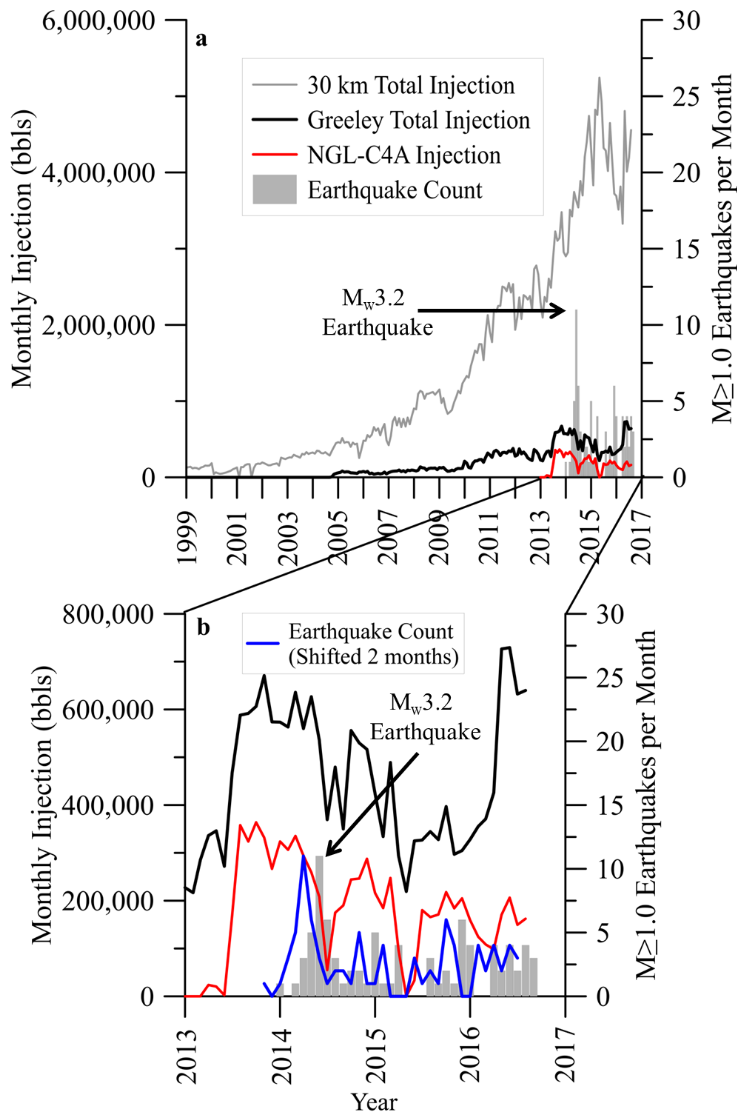

Figure 8: Injection and seismicity M>1.0 history. (a.) History of wastewater injection, into the Denver Basin combined disposal zone, within 30 km of the area of seismicity. The grey line represents the total monthly injection for all the wells; the black line is the total monthly injection for the Greeley Wells. The bar graph represents the earthquakes per month. (b.) Total monthly injection for the Greeley Wells and earthquakes per month for January 2013 through August 2016. The blue line represents the earthquakes per month shifted two months to show the approximate lag in the correlation between the injection and seismicity. Earthquake data between November 2013 and April 2015 are from *Yeck et al.* [2016].

Hydrologic parameters were needed for modeling of pore pressure generated from injection. To estimate hydrologic parameters for the injection interval, we reanalyzed step rate test data on four wells with injection intervals in the Denver Basin combined disposal zone (Figure 7a) and conducted constant-head permeameter tests on core samples from the injection interval units. The step rate test data are obtained from the *COGCC* [2016]. We took core samples from the 1UPPR-Ferch Core (Figure 7a) stored at the U.S. Geological Survey's Core Research Center [*USGS CRC,* 2016].

Step rate tests are conducted on injection wells during the well permitting process to determine the injection interval's fracture parting pressure – the pressure at which preexisting fractures extend or new fractures form within the formation. During a step rate test, pressure in the injection well is initially allowed to equilibrate to formation pressure [*Singh et al.,* 1987]. A variable rate injection test is then performed in a step rate fashion using steps of equal time length and increasing injection rate. The length of the time step is chosen such that the bottom-hole pressure is stabilized at the end of each time step, for wells near Greeley usually less than 30 minutes. Data recorded are the injection rate and well bottom-hole pressure. The injection rate versus the stabilized bottom-hole pressure data are expected to be linear with a constant slope until the fracture parting pressure is reached. Once the fracture parting pressure is reached, fractures are created and they act as higher permeability conduits for fluid and pressures are lowered, resulting in a reduced slope.

We analyzed the step rate test data from four wells, HPD Platteville #2, NGL-C11, NGL-C8A, NGL-C9B (Figure 7a), as a step-drawdown test, which is a variable rate pumping test used to determine hydrologic properties under different pumping conditions. The data are from the *COGCC* [2016] well files for the four disposal wells. Step rate and step-drawdown tests have similar procedures although one test injects (step rate test) while the other pumps (step-drawdown test). Since the two tests have a procedure of step rate injection/pumping, the same equation that solves the step-drawdown test can be used on data from the step rate test to estimate hydraulic conductivity. The sign on the pumping rate and change in hydraulic head is just reversed for injection and increasing hydraulic head.

We use the program AQTESOLV [*Duffield,* 2006] for the analysis. AQTESOLV solves for transmissivity and storativity using a modified version of the Theis method [*Theis,* 1935] for step-drawdown tests in confined aquifers; we use this method for single-well tests assuming fully penetrating wells and taking into account linear and nonlinear well losses [*Bear,* 1979 p. 374-375]:

$$\Delta h = \frac{Q}{4\pi T}[w(u) + 2S_w] + CQ^P \tag{1}$$

$$w(u) = \int_u^\infty \frac{e^{-x}}{x}dx \tag{2}$$

$$u = \frac{r^2 S}{4Tt} \tag{3}$$

where Δh is change in hydraulic head in the pumped/injected well [L], Q is pumping or injection rate [L^3 T^{-1}], T is transmissivity [L^2 T^{-1}], S_w is the wellbore skin factor [1], CQ^P is nonlinear well loss [L], $w(u)$ is the well function [1], u is a dimensionless time parameter [1], x is the variable of integration [1], r is radial distance of influence [L], S is storativity [1], and t is time [T]. The radius of the well is used for the radial distance when analyzing single-well tests in AQETSOLV. Single-well tests estimate transmissivity well, but storativity values are hard to estimate from due to the well losses [*Jacob,* 1947; *Agarwal et al.,* 1970; *Renard et al.,* 2009]. The wellbore skin factor S_w relates to the change in permeability of the formation at the borehole due to damage during drilling or well completion [*Bear,* 1979]. Positive wellbore skin factors indicate the damaged area has a lower hydraulic conductivity than the actual formation; negative wellbore skin factors indicate the damaged area has a higher hydraulic conductivity than the actual formation [*Yang and Gates,* 1997]. The well loss constant C takes into account the well's construction (e.g. screen, liner, gravel pack) and the quality of its completion.

By varying the nonlinear well loss variables, we found the transmissivity is insensitive to the nonlinear well loss. We used several skin factors during analysis to achieve the best solution. We included an anisotropy ratio, vertical hydraulic conductivity over horizontal hydraulic conductivity (K_v/K_h), of 1:10 in the analysis, which was confirmed by the constant-head permeameter testing (see section 4.2). Using the thickness of the injection interval, we calculated the hydraulic conductivity for the disposal zone in each well.

The hydraulic conductivity ranges from approximately 10^{-8} to 10^{-7} meters per second (m s^{-1}). We note that while solution (1) assumes a homogeneous aquifer, the step rate tests were conducted over the entire injection interval, which includes numerous formations of varying composition, including sandstones and carbonates. The entire injection interval, therefore, can be heterogeneous. The hydraulic conductivity results between the wells that are located across the basin are consistent.

We conducted constant-head permeameter tests on samples collected from core drilled in the DJ Basin and stored at the USGS CRC in Denver, Colorado. The core samples are from the 1 UPPR-Ferch Well (Figure 7a) that was cored through all of the geologic units of the Denver Basin combined disposal zone. We took samples from the Lyons, Wolfcamp, Ingleside, and Fountain Formations. These formations are largely sandstones, but there are some carbonates interbedded within the Wolfcamp and Ingleside Formations. The samples were picked based on previous permeability values estimated by petrophysical service companies [*USGS CRC,* 2016]. We chose samples of relatively higher permeability estimates as those intervals are where most of the injection fluid will go within the heterogeneous injection interval.

The USGS CRC cut the core samples to a diameter of 2.5 cm. We secured the ten samples in PVC pipe for testing on a Trautwein M100000 Standard Panel permeameter. We saturated the samples by allowing at least 50 milliliters (mL) of water, which is greater than 25 pore volumes, to flow through the sample. We then ran multiple constant-head tests by measuring the time for at least 20 mL of water to flow through the sample. We calculated the hydraulic conductivity of each test using a variation of Darcy's Law [*Freeze and Cherry,* 1979]:

$$K = \frac{VL}{\pi r^2 ht} \tag{4}$$

where K is hydraulic conductivity in the direction of flow [L T^{-1}], V is volume of fluid discharged [L^3], L is sample length [L], r is sample radius [L], h is the constant head difference maintained across the sample [L], and t is time [T]. The results range from 10^{-10} to 10^{-6} m s^{-1}. These values are consistent with the hydraulic conductivities used by *Belitz and Bredehoeft* [1988] to model groundwater flow in the DJ Basin aquifers. We conducted tests on three sets of samples, one from the Lyons Formation, one from the Ingleside Formation, and one from the Fountain Formation, to measure the vertical and horizontal hydraulic conductivities from the same interval. The anisotropy (K_v/K_h) was 0.16 for the Lyons sandstone samples, 0.06 for the Ingleside sandstone/carbonate samples, and 0.19 for the Fountain coarse-grained arkose samples. The disparity in anisotropy values is likely due to the differences in lithology of the three formations or natural variation between the samples. However, the difference in the anisotropy values is only within one order of magnitude.

We modeled the change in pore pressure caused by wastewater injection from the twenty-two wells within a 30 km radius of the Greeley seismicity using the USGS 3D finite difference model MODFLOW-2005. MODFLOW solves the 3D transient groundwater flow equation for hydraulic head [*McDonald and Harbaugh,* 1988]:

$$S_s \frac{\partial h}{\partial t} = \frac{\partial}{\partial x}\left(K_x \frac{\partial h}{\partial x}\right) + \frac{\partial}{\partial y}\left(K_y \frac{\partial h}{\partial y}\right) + \frac{\partial}{\partial z}\left(K_z \frac{\partial h}{\partial z}\right) + Q \tag{5}$$

where S_s is specific storage [L^{-1}]; h is hydraulic head [L]; t is time [T]; K_x, K_y, and K_z are hydraulic conductivity in the x, y, and z directions [$L\ T^{-1}$]; and Q is the volumetric flux per unit volume of sources and/or sinks [T^{-1}]. Change in hydraulic head is calculated by subtracting the head at each time step by the initial conditions (steady-state conditions). We converted the change in hydraulic head into pore pressure change using the specific weight conversion:

$$\Delta P = \gamma \Delta h \tag{6}$$

where ΔP is pore pressure change [$MLT^{-2}L^{-2}$], γ is the specific weight of water [$MLT^{-2}L^{-3}$], and Δh is hydraulic head change [L].

We created a 3D model of 100 km by 100 km by 8.6 km that captures the asymmetric nature of the Denver Basin combined disposal zone formations. The model domain is large to reduce the effect of boundary conditions on the changes caused by the injection of the wells near the center of the model domain. We assigned constant head boundaries to the east and west sides of the domain with constant heads consistent with the hydraulic head measurements given for the units in *Belitz and Bredehoeft* [1988]. This constant head condition ensures a background regional flow of the injection interval from west to east. We set a general-head boundary on the south boundary. General-head boundaries are head-dependent flux boundaries where the flux is dependent on the difference between the simulated head inside the boundary and a specified head at a certain distance beyond the boundary. The specified head are those on the southernmost part of the DJ Basin obtained from the modeling study of *Belitz and Bredehoeft* [1988]. A no-flow boundary is assigned to the north boundary since the boundary is far enough from the injection that the modeled pore pressure change caused by injection is not affected by the boundary conditions. We assigned a constant head boundary on the model top to simulate a constant water table that follows the topography at the surface of the model domain.

As a base case, we set an isotropic, homogeneous hydraulic conductivity of the Denver Basin combined disposal zone (injection interval) to 4.6 x 10^{-7} m s^{-1}. This value is on the high end of the permeameter test results, which ranged from 10^{-10} to 10^{-7} m s^{-1}, and is consistent with the step rate test as variable rate injection test analysis, which ranged from 10^{-8} to 10^{-7} m s^{-1}. *Schulze-Makuch et al.* [1999] showed that in heterogeneous systems hydraulic conductivity scales with the volume of the tested sample. Therefore, larger volume pumping (or injection) tests are a more representative estimation of the aquifer parameters than small volume permeameter tests. While there is likely lateral heterogeneity throughout the Denver Basin, the results from the step rate test analyses are consistent and cover a wide area across the basin. In addition, the hydraulic conductivities calculated from the constant-head permeameter testing are also consistent with the step rate test estimations. The consistency in the estimated values from different wells across such a wide area supports our choice to model the injection interval as a homogeneous unit.

We assigned a hydraulic conductivity of 1.6 x 10^{-10} m s^{-1} to the confining layer, the Lykins mudstone Formation, above the injection interval. We assigned a hydraulic conductivity the same as the injection interval to the top of the crystalline basement and decreased the conductivity of the basement exponentially with depth [*Manning and Ingebritsen,* 1999]. We assigned a specific storage of 10^{-7} m^{-1}, which is in the range of values estimated in the step rate test as a variable rate injection test analysis and is consistent with values in the literature for the injection intervals [*Colorado Division of Water Resources,* 1976]. We ran the model under steady-state conditions without injection to acquire initial head conditions for the transient model. The initial hydraulic heads approximate the potentiometric surface from *Belitz and Bredehoeft* [1988] of the injection interval units that is a result of steady-state regional groundwater flow modeling study.

We placed the wells in our model based on the well logs provided by the *COGCC* [2016]. We assign the injection interval of NGL-C4A to reflect the change in the injection interval following the cementation of the bottom in June 2014. We used the injection records from the COGCC to calculate the injection rate through time for each of the twenty-two wells. The injection volume and number of injection days are reported to the COGCC on a monthly basis, and we estimated the daily injection rate by dividing the injection volume by number of injection days. We ran the model from January 1, 1999 through August 31, 2016. Each of the twenty-two wells inject for at least a portion of the time.

We present the modeled pore pressure change (Figure 9a) for November 2013, when the seismicity began; June 2014 (Figure 9b), when the M_w 3.2 earthquake occurred; and August 2016 (Figure 9c), when an addition felt sequence of earthquakes occurred. Most of the seismicity occurred between two and five km below mean sea level (bmsl) (3.4 – 6.4 km below ground surface) with the majority of the earthquakes occurring at approximately 4.25 km bmsl [*Yeck et al.,* 2016] (5.6 km below ground surface). Therefore, we present the pore pressure change at four km bmsl (~5.4 km below ground surface) (Figures 9a-9c).

The earthquakes prior to June 2014 were detected using subspace detection methods applied to two regional seismic stations, >100 km from the events [*Yeck et al.,* 2016]. We assume the detected November 2013 earthquakes are in the same area of the first locatable earthquakes (June 2014) based on the waveforms matching during the subspace detection. Therefore, the November 2013 earthquakes all occur in the area where model results predicted an increase in pore pressure of approximately 0.10 MPa (Figure 9a). The June 2014 earthquakes (Figure 9b) also occur within the area of approximately 0.10 MPa of pore pressure increase. By August 2016, the area where seismicity occurs has a pore pressure increase of approximately 0.15 MPa (Figure 9c). The north-south cross-section in Figure 9d, through the area of seismicity and NGL-C4A, shows the injection interval experiences a much larger increase in pore pressure than the crystalline basement where the majority of the earthquakes occur. In addition, the increased pore pressure extends deep into the basement and to the south of the injection wells. The injection wells closest to the cross-section are indicated in Figure 9d by triangles at the surface of the model.

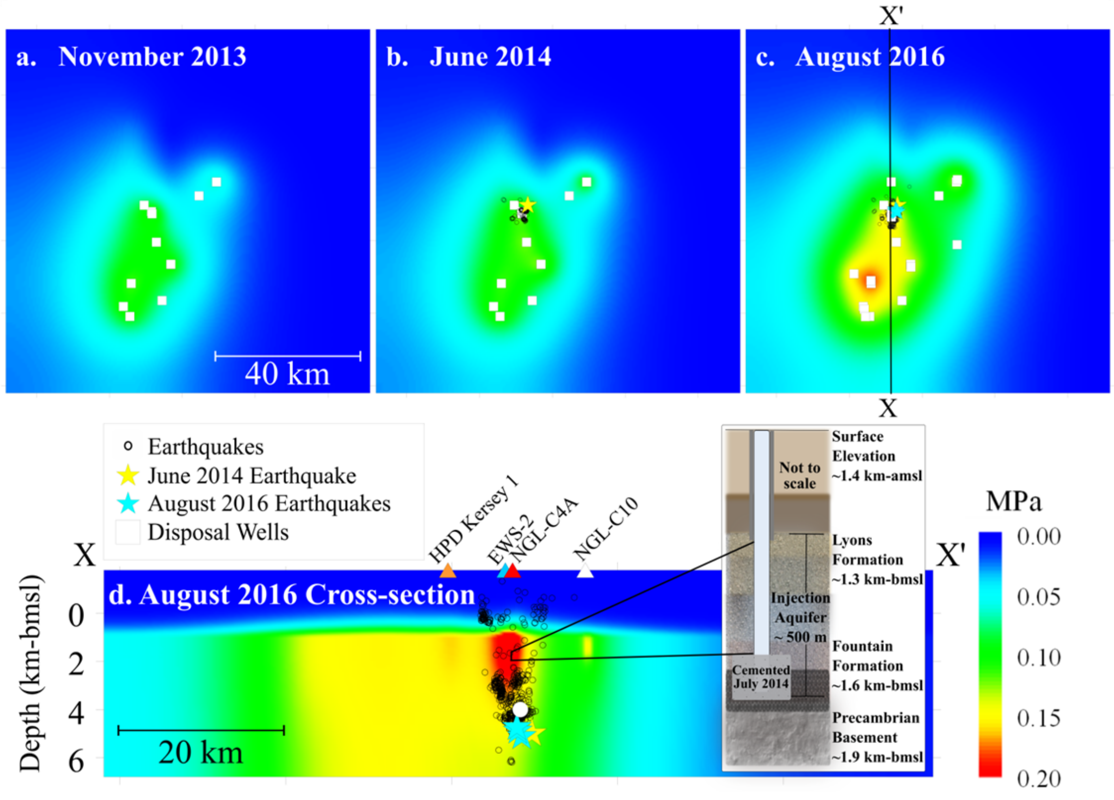

Figure 9: Modeled pore pressure results viewed at 4 km-bmsl (a. – c.). Wastewater disposal wells are labeled in white squares. (a.) Pore pressure for November 2013. (b.) June 2014 pore pressure with June 2014 earthquakes in black circles and the June 1, 2014 M_w 3.2 earthquake indicated by the yellow star. (c.) Pore pressure for August 2016 with all earthquakes since June 2014 in black circles and August 2016 felt earthquakes as blue stars. The line X-X' is the location of the cross-section in (d.). (d.) Cross-section X-X' with earthquakes projected onto the cross-section. The main grouping of seismicity starts directly below the bottom of the injection interval (~1.7-1.9 km-bsl) and extends deeper into the basement. The white dot, approximately 2 – 2.5 km below the injection interval, is the location of model estimates shown in Figures 10 and 11. Earthquake locations from June 2014 through April 2015 are from *Yeck et al.* [2016]. Surface locations of wastewater injection wells close to the cross-section are labeled with triangles. An inset of a generalized well diagram of NGL-C4A with main injection interval formations labeled is included to illustrate the Denver Basin combined disposal zone. The well diagram is modified from *Yeck et al.* [2016].

These results are from the base case scenario with mid-range hydraulic conductivity in the injection interval, no anisotropy, and no fractured (higher hydraulic conductivity) layer. We tested other scenarios during the sensitivity analysis. We performed sensitivity analyses of the model for a range of hydraulic conductivities obtained from the permeameter tests and step rate tests analysis. In addition, we ran the model with combinations of anisotropy and the presence of a high hydraulic conductivity fractured layer near NGL-C4A and across the entire basin (Figure 10), a feature inferred from the well logs and the spinner survey conducted on NGL-C4A. Model results using the lowest hydraulic conductivity values for the injection interval produced unrealistically high pore pressure changes and, therefore, are not presented. Figure 10 presents the pore pressure change at a location (shown in Figure 9d) near the majority of the earthquakes for each of the sensitivity analysis results. Excluding the highest hydraulic conductivity scenario, the pore pressure near the majority of the earthquakes increases in the sensitivity analysis to at least 0.08 MPa by November 2013 when the seismicity started.

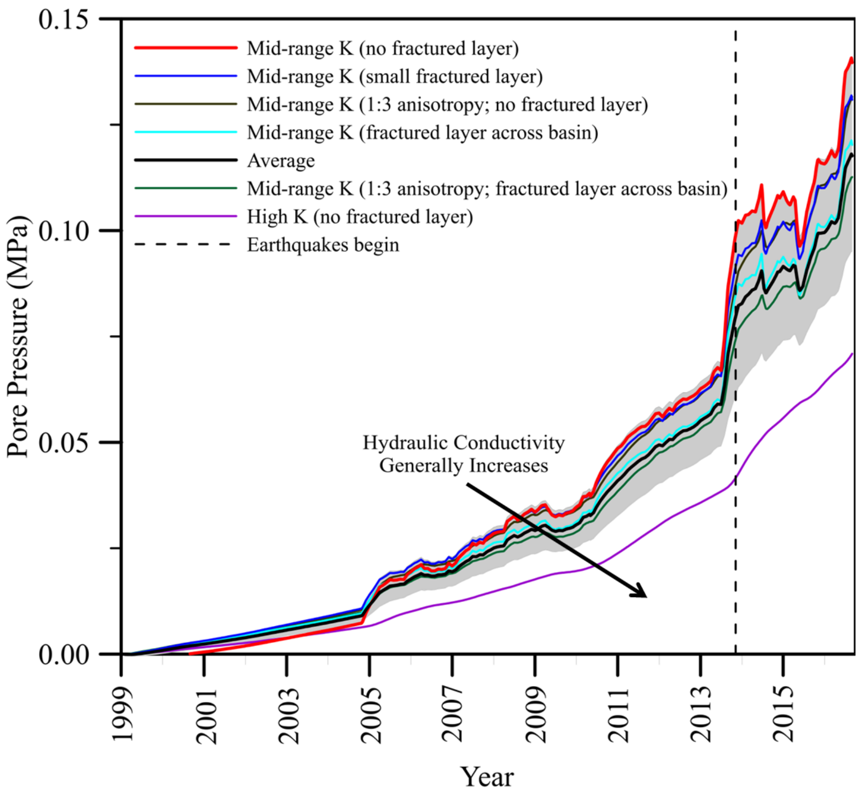

Figure 10: Pore pressure change (MPa) through time at a location in the area of seismicity, located at white dot in Figure 9d. Colored lines each represent one scenario in the sensitivity analysis. The dark black line represents the average of the pore pressure change and the grey area is +/- one standard deviation. The thicker red line is the model results shown in Figures 9 and 11. The vertical dashed line is November 2013, when seismicity began.

We also ran the model, using the base case parameters as used to attain the results shown in Figure 9, with only the Greeley Wells injecting; only NGL-C4A; and only the Far-field Wells between 15-30 km from the seismicity injecting to determine the relative contribution of these wells to the total pore pressure increase at a single location (shown in Figure 9d) near the majority of the earthquakes. The results are presented in Figure 11. Figure 11a shows a pore pressure increase of approximately 0.10 MPa in November 2013 when all wells within 30 km of radius inject. Figure 11b shows that 68% of the pore pressure increase in November 2013 is attributed to the Greeley Wells (which includes NGL-C4A), and 34% of the pore pressure increase in November 2013 is attributed to NGL-C4A alone. Figure 11c shows the pore pressure increase caused by injection at the Far-field Wells both from the modeled far-field injection and from subtracting the model results of the only Greeley Wells injecting from the results of all wells injecting (Calculated Far-field). The percentage of the modeled total pore pressure increase due to injection of the Far-field Wells is also presented in Figure 11d. The results in Figure 11c and 11d show a small difference between the modeled and calculated far-field results.

We also assess the influence of the well groupings by averaging the percentages of pore pressure increase for each well grouping's modeled results. The Far-field Well grouping's averaged percentage was calculated using the percentage difference between the all well injection model results and the only Greeley Wells injection model results. On average, the Greeley Wells (including NGL-C4A) contribute 56% of the pore pressure, NGL-C4A contributes 28% of the pore pressure, and the Far-field Wells contribute 44% of the pore pressure.

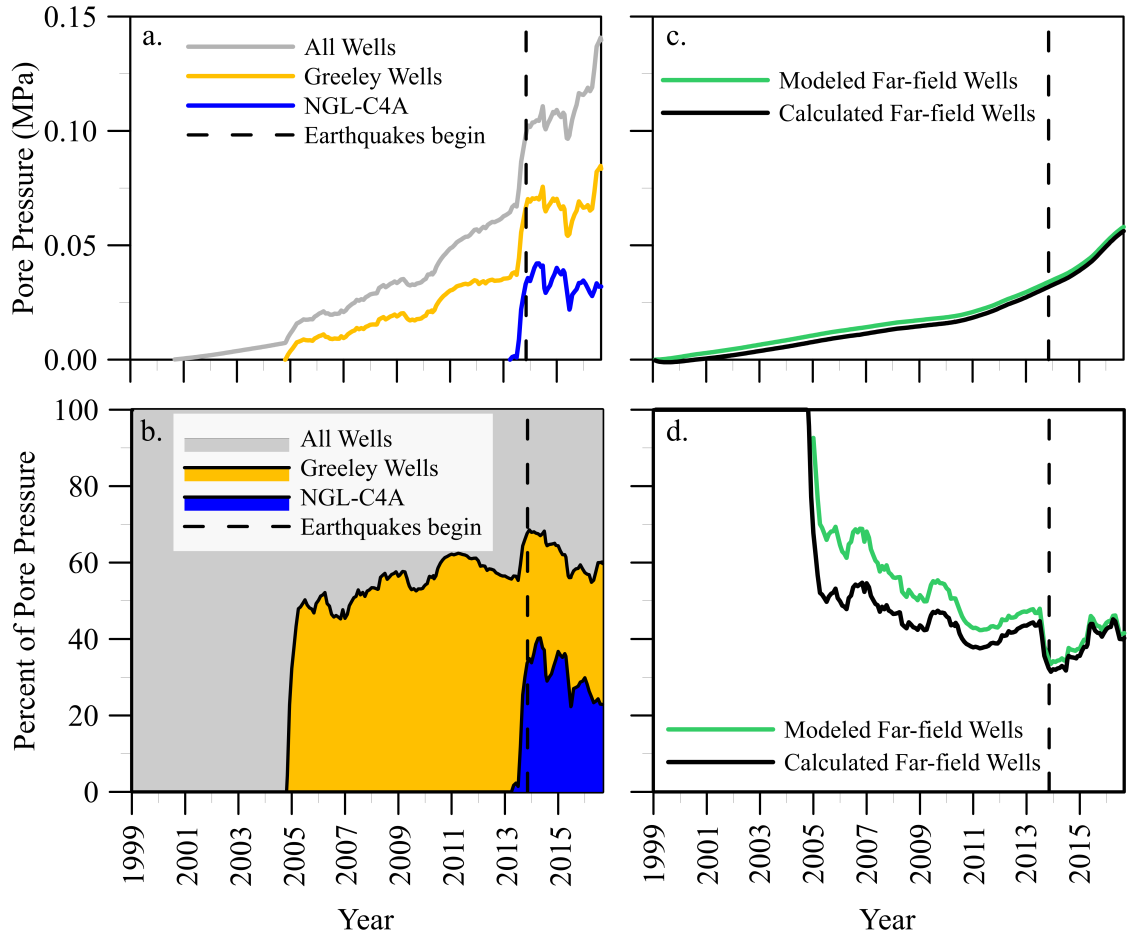

Figure 11: Well contributions to pore pressure change at a location in the area of seismicity, located at white dot in Figure 9d. (a.) Pore pressure change (MPa) through time for all wells (grey), only Greeley Wells (orange), and only NGL-C4A (blue). (b.) The percent of the total pore pressure change by well grouping. Grey represents 100% of the pore pressure change from all the wells. Orange represents the percent of the total pore pressure change from only the Greeley Wells (within 15 km). Blue represents the percent of the total pore pressure change from only NGL-C4A. (c.) Pore pressure change (MPa) through time for the far-field wells (15 – 30 km from the seismicity). The green line represents the pore pressure change results when only the injection of the far-field wells is modeled. The black line represents the pore pressure change caused by the injection of the far-field wells calculated from the difference between the modeled results for injection of all the wells and modeled results for injection of only the Greeley Wells. (d.) The percent of the total pore pressure change for the far-field wells. The vertical black dashed line is November 2013, when seismicity began.

Pore pressure modeling shows that the Greeley area seismicity began after the pore pressure increase reached approximately 0.10 MPa in the area of activity. The largest contribution to pore pressure increase, on average 56% in the area of seismicity, is from the seven Greeley Wells that are within 15 km of the seismic area. However, the wells between 15 and 30 km of the center of seismicity still contributed a substantial portion, on average 44%, of the pore pressure increase near the seismicity. Our results show not only the influence of injection on pore pressure at short distances from the earthquakes, but also the significant contribution to pore pressure change by injection at all distances modeled, up to 30 km, from the earthquakes.

Our modeling shows that pore pressure increase from injection could reach 0.15 MPa without a permeable pathway such as a fault or fractured zone. This magnitude of pore pressure increase has been shown in other studies to be sufficient to induce seismicity [*Ogwari and Horton*, 2016; *Hornbach et al.,* 2015; *Keranen et al.,* 2014]. In addition, sensitivity analysis of hydraulic conductivity shows pore pressure in the area of seismicity could increase to a level that induces earthquakes for the range of hydraulic conductivity in the area.

The local seismic network continues to detect seismicity in the area but at a low rate. Our model results indicate the pore pressure continues to increase with continued injection near the seismicity. Since over 50% of the pore pressure increase in the area of seismicity can be attributed to the Greeley Wells, a more effective approach to well modification may include reduction of injection rates at these wells. Furthermore, the Far-field Wells between 15 and 30 km from the seismicity contribute approximately 44% of the pore pressure increase. This is a significant portion of the total increase in pore pressure. An appropriate preventative mitigation action may include larger spacing between wells. Farther well spacing would reduce the number of wells within a prescribed distance such that the spatial aggregation of the injection rate would be much smaller. Mitigating induced seismicity may require hard decisions about economic and physical feasibility. A cost-benefit analysis of the number of wells, well spacing, and injection rate limitation would be necessary to examine the feasibility of various scenarios.

Seismic Data Collection at New High Rate Wells

Our seismic data collection in the NE Colorado (Greeley) area started with fives seismograph stations centered on the epicenter of the 2014 earthquake. The stations all had short period 3 component L22 sensors, one had an accelerometer, and two of the stations were telemetered to the USGS and then to IRIS. In 2016 the network was expanded to include a larger part of the Denver Basin, for a total of 16 stations. Telemetry was added to all stations. The new stations were cited near high rate disposal wells or groups of wells that had not yet experienced seismicity. All data are send in real-time by cell phone modem to the University of Colorado Boulder, and from there transmitted to the USGS in Golden and the Incorporated Research Institutions for Seismology (IRIS) data management center in Seattle. All data are immediately open and unrestricted.

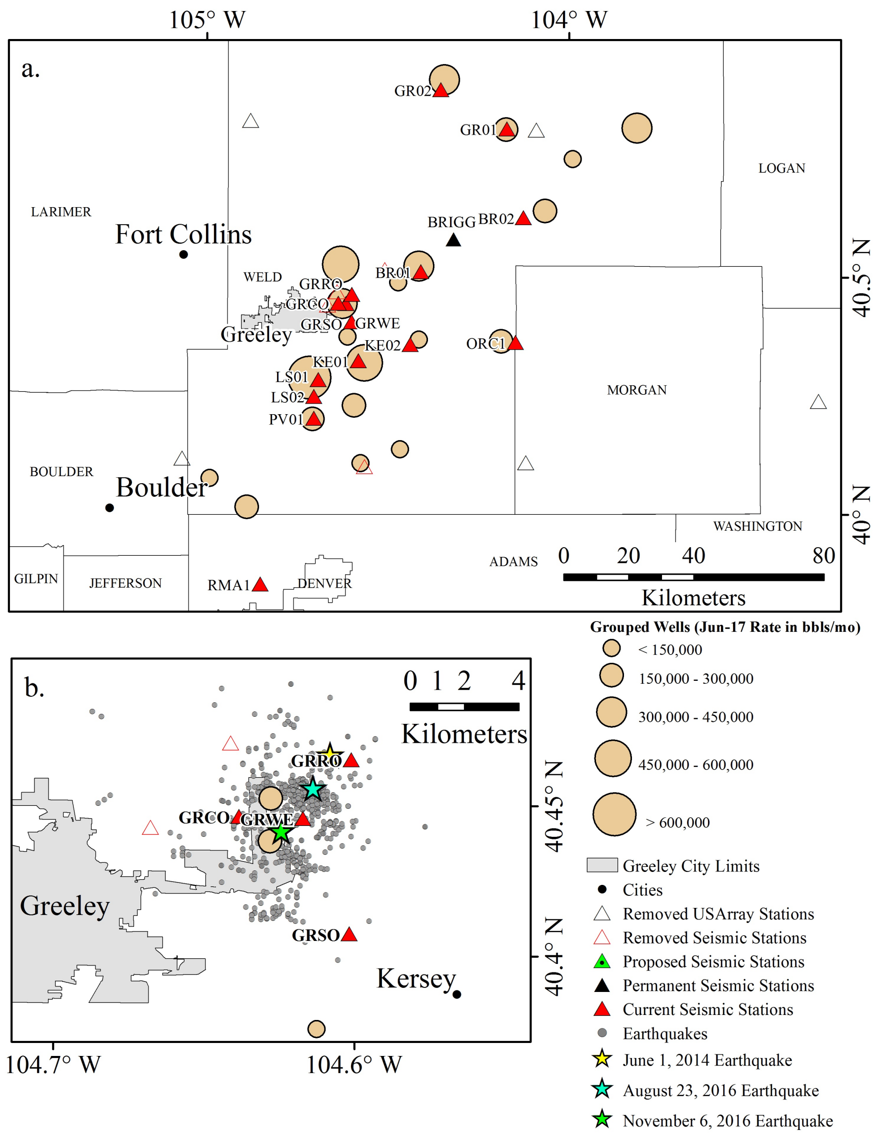

Figure 11. (a.) Seismic stations (triangles) and wastewater disposal wells (tan circles, sized by June 2017 monthly volume, wells within 5 km summed) in northeast Colorado. Seismometers currently operated by University of Colorado are red triangles, with station name marked. Stations immediately east of Greeley installed in 2014, other stations installed in summer 2016. Former USArray Transportable Array (TA) seismometer locations in open black triangles. Solid black triangle is Colorado Geological Survey station BRIGG installed in 2016. (b.) Seismicity from June 2014 to August 2016. Yellow star indicates the location of the June 1, 2014 M_w 3.2 earthquake, blue star indicates location of felt earthquakes of August 2016, green star indicates location of November 2016 earthquakes. NGL C4A is northernmost well (tan circle) in plot b, EWS2 is middle well, HPD1 is southernmost well of plot b. Sample waveforms are shown in Figure 12.

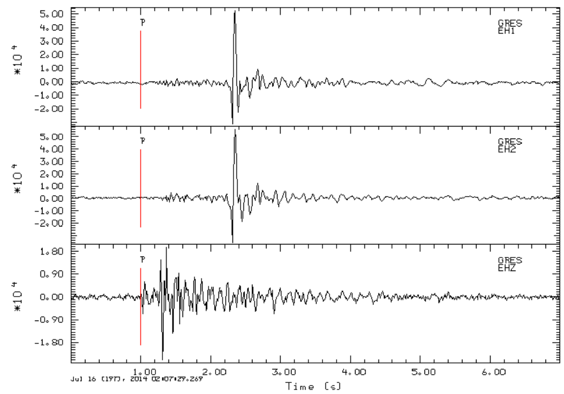

Figure 12. Example 3-component seismogram of a local earthquake recorded at station GRES, located 3 km from well C4A. Top two channels are horizontal components, bottom channel is vertical component. S waves, in this case at 2.3 s, are typically very clear. A strong arrival after P, interpreted as and S-to-P conversion at the basement-sediment contact, is often observed on the vertical component.

Publications resulting from this Award

Brown, M.R.M., and S. Ge, Small earthquakes matter in injection-induced seismicity, Geophys. Res. Lett., in press, 2018.

Brown, M.R.M., S. Ge, A. F. Sheehan, J. Nakai (2017), Evaluating the effectiveness of induced seismicity mitigation: Numerical modeling of wastewater injection near Greeley, Colorado, J. Geophys. Res. Solid Earth, 122, doi:10:1001/2017JB014456.

Nakai, J. S., A. F. Sheehan, and S. L. Bilek (2017), Seismicity of the Rocky Mountains and Rio Grande Rift from the EarthScope Transportable Array and CREST temporary seismic networks, 2008–2010, J. Geophys. Res. Solid Earth, 122, doi:10.1002/2016JB013389.

Yeck, W. L., A. F. Sheehan, H. M. Benz, M Weingarten, J Nakai, Rapid response, monitoring, and mitigation of induced seismicity near Greeley, Colorado, Seismological Research Letters, v. 87, no. 4, July/August 2016, doi:10.1785/0220150275.

Presentations at Professional meetings

Brown, M.R.M., S. Ge, and A.F. Sheehan, 2017, The Influence of Wastewater Injection Wells on Induced Seismicity in the Denver Basin Combined Disposal Zone, Weld County, Northeast Colorado, presented at 2017 12th Annual Hydrologic Sciences Research Symposium, 6-7 April.

Brown, M.R.M., S. Ge, and A.F. Sheehan, 2017, The Influence of Wastewater Injection Wells on Induced Seismicity in the Denver Basin Combined Disposal Zone, Weld County, Northeast Colorado, Abstract 2612827 presented at 2017 AAPG Annual Convention& Exhibition, Houston, TX, 2-5 April.

Brown, M.R.M., S. Ge, and A.F. Sheehan, 2016, Numerical Modeling of Wastewater Injection in the Denver Basin Combined Disposal Zone in Northeast Colorado, Abstract S53E-06 presented at 2016 American Geophysical Union Fall Meeting, San Francisco, CA, 12-16 Dec.

Brown, M.R.M., S. Ge, A.F. Sheehan, and J.S. Nakai, 2016, Numerical Modeling of Wastewater Injection and Induced Seismicity in Greeley, Colorado, Abstract 286002 presented at 2016 Geological Society of America Annual Meeting, Denver, CO, 25-28 Sept.

Brown, M.R.M., and S. Ge, 2017, Examining the role of Coulomb static stress transfer in injection-induced seismicity: a generic modeling approach, Abstract NS21A-05 presented at 2017 American Geophysical Union Fall Meeting, New Orleans, La., 11-15 Dec.

Holmes, R., K.R. Bogolub, A.F. Sheehan, and M.R.M. Brown, 2017, Induced Seismicity in Greeley, CO: The Effects of Pore Pressure on Seismic Wave Character, Abstract S23C-0837 presented at 2017 American Geophysical Union Fall Meeting, New Orleans, La., 11-15 Dec.

Nakai, J., W.L. Yeck, A.F. Sheehan, H.M. Benz, M. Weingarten. (2016) Rapid Response, Monitoring, and Mitigation of Induced Seismicity Near Greeley, Colorado. Abstract presented at 2016 Annual Conference, Groundwater Protection Council Underground Injection Control, Denver, Colo., 23-25 Feb, oral.

Presentations to Stakeholder groups

Colorado School of Mines, Heiland Lecture, October 2015, Anne Sheehan, "Induced Earthquakes in Colorado: From Classic Cases to Modern Mitigation"

April 12, 2016. Sheehan anticipated in a panel discussion on injection induced earthquakes at the law firm of Davis Graham & Stubbs in Denver.

Talk with CGS about their seismometer siting - Fall 2015, Spring 2016

Talk with USGS and COGCC about seismic monitoring in Colorado July 2017

Rocky Mountain Arsenal field trip as part of SSA meeting, April 2017. Led 50-person field trip to Rocky Mountain Arsenal to learn about history of waste injection and induced seismicity there, visited an oil and gas wastewater disposal well facility in Weld County, conducted driving tour of drilling and production operations in Weld and Boulder counties.

Presented at Morgan County Planning and Zoning Department injection well stakeholder meeting, Oct 17, 2017. Invited to present by Morgan County Planning Administrator. Presented background information and Greeley case study on induced seismicity, and answered questions. Meeting included general public, industry, planning commissioners, county commissioners, state regulators, neighboring county (Weld) director of planning services to discuss their experiences and regulations.

Data sets

1. Anne Sheehan (2016): USGS NEHRP Proposal 2016-0180 - Greeley. International Federation of Digital Seismograph Networks. Other/Seismic Network. doi:10.7914/SN/XU_2016. http://www.fdsn.org/networks/detail/XU_2016/

2. Anne Sheehan (2014): Greeley Colorado RAMP Deployment 2014. International Federation of Digital Seismograph Networks. Other/Seismic Network. doi:10.7914/SN/XU_2014

References cited

Agarwal, R.G., Al-Hussainy, R., and H.J.J. Ramey (1970), An investigation of wellbore storage and skin effect in unsteady liquid flow: I. Analytical treatment, *Society of Petroleum Engineers Journal, 10*, 279–290.

Bear, J. (1979), *Hydraulics of Groundwater*, McGraw-Hill, New York, NY.

Belitz, K., and J. D. Bredehoeft (1988), Hydrodynamics of Denver Basin: explanation of subnormal fluid pressures, *American Association of Petroleum Geologists Bulletin*, *72*(11), 1334–1359, doi:10.1306/703C999C-1707-11D7-8645000102C1865D.

Brown, M.R.M., S. Ge, A. F. Sheehan, J. Nakai, Evaluating the effectiveness of induced seismicity mitigation: Numerical modeling of wastewater injection near Greeley, Colorado, J. Geophys. Res., 122, doi:10.1002/2017JB014456.

COGCC (2016), Colorado Oil & Gas Conservation Commission, http://cogcc.state.co.us/data.html#/cogis

Colorado Division of Water Resources (1976), *Ground Water Resources of the Bedrock Aquifers of the Denver Basin, Colorado*, Department of Natural Resources, Denver, CO.

Duffield, G. M. (2006), *AQTESOLV for Windows Version 4 User's Guide*, HydroSOLVE, Inc., Reston, VA.

Freeze, R. A., and J. A. Cherry (1979), *Groundwater*, Prentice-Hall, Inc., Englewood Cliffs, NJ.

Healy, J. H. (1966). Geophysical and geological investigations relating to earthquakes in the Denver area, Colorado (No. 66-60). US Geological Survey

Healy, J. H., W. W. Rubey, D. T. Griggs, and C. B. Raleigh (1968), The Denver Earthquakes, *Science*, *161*(3848), 1301–1310.

Herrmann, R. (2016), North America Moment Tensor 1995–2016, accessed May 11, 2017, from St. Louis University web site:, http://www.eas.slu.edu/eqc/eqc_mt/MECH.NA/20140601033521/index.html, (Updated December 7, 2015).

Keranen, K. M., M. Weingarten, G. A. Abers, B. A. Bekins, and S. Ge (2014), Induced earthquakes. Sharp increase in central Oklahoma seismicity since 2008 induced by massive wastewater injection, *Science*, *345*(6195), 448–451, doi:10.1126/science.1255802.

Lomax, A., J. Virieux, P. Volant, and C. Berge-Thierry (2000), Probabilistic earthquake location in 3D and layered models - Introduction of a Metropolis-Gibbs method and comparison with linear locations, *Adv. Seism. Event Locat.*, 101–134, doi:10.1007/978-94-015-9536-0_5.

Lomax, A., A. Michelini, and A. Curtis (2009), Earthquake location, direct, global-search methods, *Encycl. Complex. Syst. Sci.*, 2449–2473, doi:10.1007/978-0-387-30440-3.

Manning, C. E., and S. E. Ingebritsen (1999), Permeability of the continental crust: Implications of geothermal data and metamorphic systems, *Reviews of Geophysics*, *37*(1), 127–150, doi:10.1029/1998RG900002.

Nakai, J.S., A.F. Sheehan, and S.L. Bilek (2017), Seismicity of the rocky mountains and Rio Grande Rift from the EarthScope Transportable Array and CREST temporary seismic networks, 2008-2010, *Journal of Geophysical Research Solid Earth, 122*, doi:10.1002/2016JB013389.

Ogwari, P.O., and S.P. Horton (2016), Numerical model of pore-pressure diffusion associated with the initiation of the 2010-2011 Guy-Greenbrier, Arkansas earthquakes, *Geofluids, 16*, 954-970, doi:10.111/gfl.12198.

Singh, P.K., R.G. Agarwal, and L.D. Krase (1987), Systematic Design and Analysis of Step-Rate Test to Determine Formation Parting Pressure, *Society of Petroleum Engineers*, *SPE 16798*(September), 491–503.

USGS CRC (2016), USGS Core Research Center, https://geology.cr.usgs.gov/crc/

Weingarten, M. and S. Ge (2015), Hydrogeologic Modeling Aimed at Optimizing Injection Well Operation in a Hypothetical Multi-Injection Well Reservoir: Implications for Induced Seismicity, Abstract S13B-2820 presented at 2015 Fall Meeting, AGU, San Francisco, Calif., 14-18 Dec.

Weingarten, M., S. Ge, J. W. Godt, B. A. Bekins, and J. L. Rubinstein (2015), High-rate injection is associated with the increase in U.S. mid-continent seismicity, *Science*, *348*(6241), 1336–1340, doi:10.1126/science.aab1345.

Wiemer, S. (2001), A software package to analyse seismicity: ZMAP, *Seism. Res. Lett.*, *72*, 373–382.

Wiemer, S., and M. Wyss (2000), Minimum Magnitude of Completeness in Earthquake Catalogs: Examples from Alaska, the Western United States, and Japan, *Bulletin of the Seismological Society of America*, *90*(4), 859–869, doi:10.1785/0119990114.

Woessner, J., and S. Wiemer (2005), Assessing the Quality of Earthquake Catalogues: Estimating the Magnitude of Completeness and Its Uncertainty, *Bulletin of the Seismological Society of America*, *95*(2), 684–698, doi:10.1785/0120040007.

Yang, Y.J., and T.M. Gates (1997), Wellbore skin effect in slug-test data analysis for low permeability geologic materials, *Groundwater, 35*(6), 931-937.

Yeck, W. L., A. F. Sheehan, H. M. Benz, M. Weingarten, and J. Nakai (2016), Rapid Response, Monitoring, and Mitigation of Induced Seismicity near Greeley, Colorado, *Seismological Research Letters*, *87*(4), 837–847, doi:10.1785/0220150275.

Yeck, W. L., G. P. Hayes, D. E. McNamara, J. L. Rubinstein, W. D. Barnhart, P. S. Earle, and H. M. Benz (2017), Oklahoma experiences largest earthquake during ongoing regional wastewater injection hazard mitigation efforts, *Geophysical Research Letters*, *44*, 711–717, doi:10.1002/2016GL071685.

Appendix 1: Seismograph stations in NE Colorado

Network XU Greeley, CO USGS NEHRP Proposal (2016-2018)

Station Name	Latitude	Longitude	Elevation (m)	Install Date	Demobilization Date	Sensor Model	Digitizer Model	Telemetry Start Date	Notes	Location
BR01	40.5181	-104.41	1437	5/24/16	3/12/18	Guralp CMG40T	Reftek 130	5/24/16		Briggsdale Southeast, CO
BR02	40.626	-104.126	1576	8/13/16		Guralp CMG40T	Reftek 130	8/13/16		Briggsdale East, CO
GR01	40.8122	-104.172	1553	6/3/16		Guralp CMG40T	Reftek 130	6/3/16		Grover South, CO, USA
GR02	40.8939	-104.354	1576	8/13/16		Mark Products L22	Reftek 130	8/13/16		Grover West, CO, USA
GRCO	40.4466	-104.638	1427	6/25/16	10/19/17	Guralp CMG3T	Reftek 130		Swapped L22 for CMG-3T on 6/25/2017	Chill station, CO, USA
	40.4466	-104.638	1427	10/19/17		Guralp CMG40T	Reftek 130		Swapped CMG-3T for 40T on 10/19/2018	Chill station, CO, USA
GRRO	40.4654	-104.601	1430	6/30/16	7/7/18	Mark Products L22	Reftek 130	6/30/16		Greeley Roth Farm, CO
	40.4654	-104.601	1430	7/7/18		Guralp CMG40T	Reftek 130			Greeley Roth Farm, CO
GRSO	40.4076	-104.602	1412	7/12/17		Guralp CMG40T	Reftek 130		Swapped L22 for CMG-40T on 7/12/17	Greeley South, CO, USA
GRWE	40.4459	-104.617	1423	7/17/17		Guralp CMG40T	Reftek 130		Swapped L22 for CMG-40T on 7/17/17	Greeley Well, CO, USA
HU01	40.1021	-104.565	1535	5/26/16	7/7/16	Guralp CMG40T	Reftek 130			Hudson West, CO, USA
KE01	40.3255	-104.583	1475	5/20/16	6/23/17	Mark Products L22	Reftek 130	5/20/16		Kersey, CO, USA
	40.3255	-104.583	1475	6/23/17		Guralp CMG3T	Reftek 130			Kersey, CO, USA
KE02	40.3598	-104.439	1386	6/17/16		Guralp CMG40T	Reftek 130	6/17/16		Kersey East, CO, USA
LS01	40.2856	-104.694	1474	5/13/16		Mark Products L22	Reftek 130	5/13/16		La Salle South, CO
LS02	40.2506	-104.706	1530	6/21/16	7/18/17	Mark Products L22	Reftek 130	6/21/16		Lasalle West, CO, USA
	40.2506	-104.706	1530	7/18/17		Guralp CMG3T	Reftek 130			Lasalle West, CO, USA
ORC1	40.364	-104.148	1386	11/8/16		Guralp CMG40T	Reftek 130	11/8/16		Orchard, CO, USA
PV01	40.204	-104.706	1518	5/17/16		Guralp CMG40T	Reftek 130	5/17/16		Platteville Wells, CO
RMA1	39.8533	-104.854	1585	8/12/16		Guralp CMG40T	Reftek 130	8/12/16		Rocky Mountain NE, CO

*Continued stations in gray **Stations with recent sensor swaps outlined

Network XU Greeley, Colorado RAMP deployment (2014-2015)

Station Name	Latitude	Longitude	Elevation (m)	Install Date	Demobilization Date	Sensor Model	Digitizer Model	Telemetry Start Date	Notes	Location
GRCO	40.4466	-104.638	1427	7/17/14	6/25/17	Mark Products L22	Reftek 130	on/before 5/19/16	Swapped L22 for CMG-3T on 6/25/17	Chill station, CO, USA
GREP	40.4712	-104.641	1443	6/3/14	4/28/15	Mark Products L22	Reftek 130			Greeley Epicenter, CO
GRES	40.443	-104.668	1431	6/4/14	6/30/16	Mark Products L22	Reftek 130	6/5/14		Greeley East, CO, USA
GRNE	40.5169	-104.509	1458	6/4/14	6/20/15	Mark Products L22	Reftek 130			Gill, CO, USA
GRNW	40.5451	-104.791	1427	6/4/14	6/20/14	Mark Products L22	Reftek 130			Eaton, CO, USA
GRSO	40.4076	-104.602	1412	6/5/14	7/12/17	Mark Products L22	Reftek 130	on/before 5/19/16	Swapped L22 for CMG-40T on 7/12/17	Greeley South, CO
GRWE	40.4459	-104.617	1421	6/20/14	7/17/18	Mark Products L22	Reftek 130	7/19/14	Swapped L22 for CMG-40T on 7/17/17	Greeley Well, CO, USA

Appendix 2: Outcrop Sample Permeameter Results

Constant-Head permeameter test results from tests done using a Trautwein M100000 Standard Panel permeameter on samples from the Horsetooth Reservoir (HR samples) and Owl Canyon, CO (OC samples) areas. First, the samples were saturated with 30-50 mililiters (mL) of water. Second, up to 10 tests were run using approximately 20 mL of water each. All test were completed using tap water at room temperature. cm = centimeter; mL = mililiter; s = seconds; psi = pounds per square inch; SAT = saturation part of tests. In sample names, letter abbreviations and numbers give the sample locations; and V and H in sample names represents vertical or horizontal samples. Data provided by Megan R.M. Brown, University of Colorado Boulder; please also acknowledge Mazi-Mathias Onyeali, University of Colorado Boulder. Citation: Brown, M.R.M., S. Ge, A.F. Sheehan, and J.S. Nakai (2017), Evaluating the Effectiveness of Induced Seismicity Mitigation: Numerical Modeling of Wastewater Injection near Greeley, Colorado, Journal of Geophysical Research Solid Earth,122, 6569-6582, doi: 10.1002/2017JB014456

Sample	Test	Diameter (cm)	Area (cm^2)	Length (cm)	Total Volume (mL)	Time (days)	Time (minutes)	Time (s)	Pressure (psi)	head (cm)	Q (cm^3/s)	K (cm/s)	K (m/s)
OC1-1	1	2.7	5.7	4.2	120.42		10.41	624.42	9.4	660.89	0.193	2.14E-04	2.14E-06
Ingleside Formation	2				106.68		7.71	462.84	9.6	674.95	0.230	2.51E-04	2.51E-06
	3				120.42		9.30	557.94	10	703.07	0.216	2.25E-04	2.25E-06
	4				138.02		9.25	554.85	10.1	710.10	0.249	2.57E-04	2.57E-06
	5				113.60		8.91	534.30	9.4	660.89	0.213	2.36E-04	2.36E-06
	6				115.87		10.09	605.49	9.4	660.89	0.191	2.12E-04	2.12E-06
	7				112.36		8.99	539.40	9.4	660.89	0.208	2.31E-04	2.31E-06
	8				125.528		8.79	527.4	10	703.07	0.238	2.48E-04	2.48E-06
	9				123.824		7.98	478.8	10	703.07	0.259	2.70E-04	2.70E-06
	10				126.096		7.73	463.8	10.1	710.1007	0.272	2.81E-04	2.81E-06
HR1-3H	SAT	2.7	5.7	3.3	72.704		6	360	10.1	710.1007	0.202	1.64E-04	1.64E-06
Fountain Formation	1				33.98		3	180	10.1	710.1007	0.189	1.53E-04	1.53E-06
	2				34.08		4	240	10.1	710.1007	0.142	1.15E-04	1.15E-06
	3				34.08		3.62	217.2	10.1	710.1007	0.157	1.27E-04	1.27E-06
	4				34.08		3.57	214.2	10.1	710.1007	0.159	1.29E-04	1.29E-06
HR1-4	SAT	2.7	5.7	3.2	97.028	3.82	5501	330060	10.1	710.1007	2.94E-04	2.31E-07	2.31E-09
Fountain Formation	1				45.44	2.00	2876	172560	10.1	710.1007	2.63E-04	2.07E-07	2.07E-09
	2				45.44	2.19	3148	188880	10.1	710.1007	2.41E-04	1.89E-07	1.89E-09
	3				75.544	3.69	5313	318780	10.1	710.1007	2.37E-04	1.87E-07	1.87E-09
	4				28.4	1.34	1933	115980	10.1	710.1007	2.45E-04	1.93E-07	1.93E-09
	5				51.688	1.98	2856	171360	10.1	710.1007	3.02E-04	2.37E-07	2.37E-09
	6				105.648	3.84	5525	331500	10.1	710.1007	3.19E-04	2.51E-07	2.51E-09
	7				55.096	2.04	2944	176640	10.1	710.1007	3.12E-04	2.45E-07	2.45E-09
	8				31.14	1.11	1594	95640	10.1	710.1007	3.26E-04	2.56E-07	2.56E-09
	9				103.376	3.82	5496	329760	10.1	710.1007	3.13E-04	2.47E-07	2.47E-09
	10				56.8	2.07	2974	178440	10.1	710.1007	3.18E-04	2.51E-07	2.51E-09
HR1-3V	SAT	2.7	5.7	3.2	63.31	1.24	1784	107040	10.1	710.1007	5.91E-04	4.66E-07	4.66E-09
Fountain Formation	1				25.324	0.94	1358	81480	10.1	710.1007	3.11E-04	2.45E-07	2.45E-09
	2				36.912	3.03	4364	261840	10.1	710.1007	1.41E-04	1.11E-07	1.11E-09
	3				28.246	3.17	4560	273600	10.1	710.1007	1.03E-04	8.13E-08	8.13E-10
	4				37.986	4.71	6777	406620	10.1	710.1007	9.34E-05	7.35E-08	7.35E-10
	5				23.376	3.33	4789	287340	10.1	710.1007	8.14E-05	6.40E-08	6.40E-10
	6				34.09	5.88	8474	508440	10.1	710.1007	6.70E-05	5.28E-08	5.28E-10
	7				46.265	9.87	14206	852360	10.1	710.1007	5.43E-05	4.27E-08	4.27E-10
	8				19.967	3.14	4526	271560	10.1	710.1007	7.35E-05	5.79E-08	5.79E-10

Appendix 3. Core Sample constant-head permeameter test results

Constant-Head permeameter test results from tests done using a Trautwein M100000 Standard Panel permeameter on samples from CRC library code E053. First, the samples were saturated with 30-50 mililiters (mL) of water. Second, up to 10 tests were run using approximately 20 mL of water each. All test were completed using tap water at room temperature. cm = centimeter; mL = mililiter; s = seconds; psi = pounds per square inch; SAT = saturation part of tests. Number in sample name is the depth the same was taken from (in feet) and V and H in sample names represents vertical or horizontal samples. Data provided by Megan R.M. Brown, University of Colorado Boulder; please also acknowledge Mazi-Mathias Onyeali, University of Colorado Boulder. Citation: Brown, M.R.M., S. Ge, A.F. Sheehan, and J.S. Nakai (2017), Evaluating the Effectiveness of Induced Seismicity Mitigation: Numerical Modeling of Wastewater Injection near Greeley, Colorado, Journal of Geophysical Research Solid Earth,122, 6569-6582, doi: 10.1002/2017JB014456

Sample	Test	Diameter (cm)	Area (cm^2)	Length (cm)	Annulus Initial (mL)	Annulus Final (mL)	Pipet Initial (mL)	Pipet Final (mL)	Total Volume (mL)	Time (minutes)	Time (s)	Pressure (psi)	head (cm)	Volumetric Flux Q (cm^3/s)	Hydraulic Conductivity K (cm/s)	Hydraulic Conductivity K (m/s)
9175H	SAT	2.5	4.9	3.6	2.00	22.50	1.90	22.45	99.89	32.72	1963.2	10.1	710.1	5.09E-02	5.25E-05	5.25E-07
	1				0.30	13.40	0.30	13.30	63.70	29.38	1762.8	10.1	710.1	3.61E-02	3.73E-05	3.73E-07
	2				0.50	20.70	0.40	20.60	98.37	41.83	2509.8	10.1	710.1	3.92E-02	4.05E-05	4.05E-07
	3				0.10	18.70	0.10	18.60	90.48	35.09	2105.4	10.1	710.1	4.30E-02	4.44E-05	4.44E-07
	4				0.00	14.60	0.00	14.50	71.00	30.05	1803	10.2	717.1	3.94E-02	4.03E-05	4.03E-07
	5				0.40	17.60	0.40	17.50	83.66	33.71	2022.6	10.1	710.1	4.14E-02	4.27E-05	4.27E-07
	6				0.20	19.40	0.20	19.40	93.50	32.58	1954.8	10.1	710.1	4.78E-02	4.94E-05	4.94E-07
	7				0.20	14.60	0.20	14.50	70.03	27.97	1678.2	10.1	710.1	4.17E-02	4.31E-05	4.31E-07
	8				0.00	12.20	0.00	12.10	59.31	30.29	1817.4	10.1	710.1	3.26E-02	3.37E-05	3.37E-07
	9				0.10	13.60	0.00	13.60	65.85	37.88	2272.8	10.1	710.1	2.90E-02	2.99E-05	2.99E-07
	10				0.00	12.90	0.00	12.80	62.72	37.01	2220.6	10.1	710.1	2.82E-02	2.92E-05	2.92E-07
9175V	1	2.5	4.9	3.3	0.20	7.75	0.20	7.77	36.79	109.91	6594.6	10.2	717.1	5.58E-03	5.23E-06	5.23E-08
	2				8.15	16.20	8.10	16.20	39.25	104.41	6264.6	10.2	717.1	6.27E-03	5.87E-06	5.87E-08
	3				16.30	20.90	16.25	20.80	22.35	74.44	4466.4	10.2	717.1	5.00E-03	4.69E-06	4.69E-08
	4				0.00	0.00	0.60	21.30	20.70	64.23	3853.8	10.1	710.1	5.37E-03	5.09E-06	5.09E-08
	5				0.00	0.00	0.20	20.55	20.35	59.5	3570	10.1	710.1	5.70E-03	5.40E-06	5.40E-08
	6				0.00	4.90	0.00	4.80	23.76	51.84	3110.4	10.1	710.1	7.64E-03	7.23E-06	7.23E-08
	7				4.90	10.70	4.80	10.60	28.25	62.11	3726.6	10.1	710.1	7.58E-03	7.18E-06	7.18E-08
	8				10.80	16.20	10.70	16.10	26.30	59.16	3549.6	10.1	710.1	7.41E-03	7.01E-06	7.01E-08
	9				16.25	21.50	16.20	21.40	25.52	59.34	3560.4	10.1	710.1	7.17E-03	6.79E-06	6.79E-08
	10				0.20	6.50	0.20	6.50	30.68	68.66	4119.6	10.1	710.1	7.45E-03	7.05E-06	7.05E-08
9203H	SAT	2.5	4.9	2.2	0.30	5.80	0.30	5.75	26.74	992	59520	10.1	710.1	4.49E-04	2.83E-07	2.83E-09
	SAT				5.80	13.20	5.75	13.20	36.09	4847	290820	10.1	710.1	1.24E-04	7.83E-08	7.83E-10
	SAT_Total				0.30	13.20	0.30	13.20	62.82	5839	350340	10.1	710.1	1.79E-04	1.13E-07	1.13E-09
	1				13.20	21.20	13.20	21.10	38.86	5920	355200	10.1	710.1	1.09E-04	6.90E-08	6.90E-10
	2				0.00	16.50	0.00	16.40	80.26	13934	836040	10.1	710.1	9.60E-05	6.06E-08	6.06E-10
	3				0.00	6.60	0.00	6.50	32.04	5615	336900	10.1	710.1	9.51E-05	6.00E-08	6.00E-10
	4				6.60	12.50	6.50	12.40	28.73	4815	288900	10.1	710.1	9.95E-05	6.28E-08	6.28E-10
	5				12.50	19.20	12.40	19.10	32.63	5306	318360	10.1	710.1	1.02E-04	6.47E-08	6.47E-10
	6				4.10	8.10	4.10	8.10	19.48	1179	70740	10.1	710.1	2.75E-04	1.74E-07	1.74E-09
9463H	SAT	2.5	4.9	3.6	1.50	8.40	1.50	8.40	39.19	7231	433860	10.1	710.1	9.03E-05	9.33E-08	9.33E-10
	1				8.40	14.50	8.40	14.50	34.65	11593	695580	10.1	710.1	4.98E-05	5.14E-08	5.14E-10
	2				14.50	21.50	14.50	12.50	30.76	8523	511380	10.1	710.1	6.02E-05	6.21E-08	6.21E-10
	3				0.10	10.80	0.10	10.80	60.78	8720	523200	10.1	710.1	1.16E-04	1.20E-07	1.20E-09
	4				10.80	21.20	10.80	21.20	59.07	5732	343920	10.1	710.1	1.72E-04	1.77E-07	1.77E-09
	5				0.00	6.00	0.00	6.00	34.08	2823	169380	10.1	710.1	2.01E-04	2.08E-07	2.08E-09
	6				6.00	13.90	6.00	13.90	44.87	2875	172500	10.1	710.1	2.60E-04	2.69E-07	2.69E-09
	7				0.10	7.50	0.10	7.50	42.03	2855	171300	10.1	710.1	2.45E-04	2.53E-07	2.53E-09
	8				7.50	14.60	7.50	14.60	40.33	4327	259620	10.1	710.1	1.55E-04	1.60E-07	1.60E-09
	9				14.60	21.00	14.60	21.00	36.35	4399	263940	10.1	710.1	1.38E-04	1.42E-07	1.42E-09
	10				0.50	10.80	0.50	10.80	58.50	7316	438960	10.1	710.1	1.33E-04	1.38E-07	1.38E-09
9463V	SAT	2.5	4.9	4.0	3.00	14.20	3.00	14.20	54.54	5814	348840	10.1	710.1	1.56E-04	1.79E-07	1.79E-09
	1				14.20	21.10	14.20	21.10	33.60	4248	254880	10.1	710.1	1.32E-04	1.51E-07	1.51E-09
	2				0.30	12.40	0.30	12.40	58.93	8837	530220	10.1	710.1	1.11E-04	1.28E-07	1.28E-09
	3				12.40	17.70	12.40	17.70	25.81	4241	254460	10.1	710.1	1.01E-04	1.16E-07	1.16E-09
	In Progress															
9536H	SAT	2.5	4.9	3	12.80	24.40	12.70	24.30	56.49	18.65	1119	10.1	710.1	5.05E-02	4.34E-05	4.34E-07
	1				0.70	8.20	0.70	8.10	36.43	16.58	994.8	10.1	710.1	3.66E-02	3.15E-05	3.15E-07
	2				8.50	24.40	8.50	24.30	77.33	34.41	2064.6	10.1	710.1	3.75E-02	3.22E-05	3.22E-07
	3				0.80	16.55	0.75	16.50	76.70	30.16	1809.6	10.1	710.1	4.24E-02	3.65E-05	3.65E-07
	4				0.90	17.05	0.90	17.00	78.60	33.52	2011.2	10.1	710.1	3.91E-02	3.36E-05	3.36E-07
	5				0.50	20.90	0.50	20.80	99.25	40.41	2424.6	10.1	710.1	4.09E-02	3.52E-05	3.52E-07
	6				0.40	16.90	0.40	16.80	80.26	31.66	1899.6	10.1	710.1	4.22E-02	3.64E-05	3.64E-07
	7				0.40	20.60	0.40	20.50	98.27	40.89	2453.4	10.1	710.1	4.01E-02	3.45E-05	3.45E-07
	8				0.40	13.90	0.40	13.80	65.65	25.8	1548	10.1	710.1	4.24E-02	3.65E-05	3.65E-07
	9				0.40	13.00	0.40	12.90	61.26	22.21	1332.6	10.1	710.1	4.60E-02	3.96E-05	3.96E-07
	10				0.40	12.50	0.40	12.40	58.83	21.46	1287.6	10.1	710.1	4.57E-02	3.93E-05	3.93E-07
9878.5V	SAT	2.5	4.9	2.3	1.70	11.40	1.70	11.40	47.24	135.6	8136	10.1	710.1	5.81E-03	3.83E-06	3.83E-08
	1				0.50	7.95	0.50	7.90	36.23	469.33	28159.8	10.1	710.1	1.29E-03	8.49E-07	8.49E-09
	2				0.00	15.00	0.00	15.00	73.05	879	52740	10.1	710.1	1.39E-03	9.14E-07	9.14E-09
	3				0.00	9.70	0.00	9.70	47.24	468	28080	10.1	710.1	1.68E-03	1.11E-06	1.11E-08
	4				0.00	20.20	0.00	20.10	98.27	1086	65160	10.1	710.1	1.51E-03	9.95E-07	9.95E-09
	5				0.00	5.15	0.00	5.10	25.03	268	16080	10.1	710.1	1.56E-03	1.03E-06	1.03E-08
	6				0.00	18.80	0.00	18.70	91.46	1161	69660	10.1	710.1	1.31E-03	8.66E-07	8.66E-09
	7				0.00	7.35	0.00	7.30	35.74	446	26760	10.1	710.1	1.34E-03	8.81E-07	8.81E-09
	8				0.00	15.90	0.00	15.80	77.33	1068	64080	10.1	710.1	1.21E-03	7.96E-07	7.96E-09
	9				0.00	6.00	0.00	5.90	29.12	379	22740	10.1	710.1	1.28E-03	8.45E-07	8.45E-09
	10				6.30	14.80	6.30	14.70	41.30	384	23040	10.1	710.1	1.79E-03	1.18E-06	1.18E-08